The Response of the Antarctic Oscillation to Increasing and Stabilized Atmospheric CO_2

WENJU CAI AND PETER. H. WHETTON

CSIRO Atmospheric Research, Aspendale, Victoria, Australia

DAVID J. KAROLY

School of Mathematical Sciences, Monash University, Victoria, Australia

(Manuscript received 6 June 2002, in final form 14 October 2002)

ABSTRACT

Recent results from greenhouse warming experiments, most of which follow the Intergovernmental Panel on Climate Change (IPCC) IS92a scenario, have shown that under increasing atmospheric CO_2 concentration, the Antarctic Oscillation (AAO) exhibits a positive trend. However, its response during the subsequent CO_2 stabilization period has not been explored. In this study, it is shown that the upward trend of the AAO reverses during such a stabilization period. This evolution of an upward trend and a subsequent reversal is present in each ensemble of three greenhouse simulations using three versions of the CSIRO Mark 2 coupled climate model. The evolution is shown to be linked with that of surface temperature, which also displays a corresponding trend and reversal, incorporating the well-known feature of interhemispheric warming asymmetry with smaller warming in the Southern Hemisphere (smaller as latitude increases) than that in the Northern Hemisphere during the transient period, and vice versa during the stabilization period. These results indicate that once CO_2 concentration stabilizes, reversal of the AAO trend established during the transient period is likely to be a robust feature, as it is underpinned by the likelihood that latitudinal warming differences will reduce or disappear. The implication is that climatic impacts associated with the AAO trend during the transient period may be reversible if CO_2 stabilization is achieved.

1. Introduction

Analyses of observations over the last several decades suggest that the leading mode of variability of mean sea level pressure (MSLP) or 500-hPa geopotential height (Z500) modes in the mid- to high latitudes are the annular modes (Mo and White 1985; Mo and Ghil 1987; Karoly 1990, 1995; Kidson and Sinclair 1995; Watterson 2000; Thompson and Wallace 1998, 2000; Hurrell 1995). These modes have been referred to as the Arctic Oscillation (AO) for the Northern Hemisphere (NH) and the Antarctic Oscillation (AAO) for the Southern Hemisphere (SH). Thompson and Wallace (2000) and suggest that the AAO and the AO are dynamically similar, and show that there have been trends in these two modes over the past few decades with decreasing MSLP over the polar latitudes and increasing pressure in midlatitudes.

The forcing of the AO and AAO trends has received considerable attention. Thompson and Solomon (2002) and Sexton (2001) provide observational and modeling evidence that the AAO trend is consistent with stratospheric ozone loss over the past few decades. There has also been considerable interest in the response of these modes to greenhouse warming. Based on model simulations, Shindell et al. (1999) show that the observed AO trend can be attributed to greenhouse gas–induced warming, but they also find that such a response only exists in simulations with enhanced resolution in the stratosphere. Other studies indicate that the response of the AO varies significantly from one climate model to another (Kushner et al. 2001). In Fyfe et al. (1999), which uses a relatively coarse resolution in the stratosphere, the trend of the AO is simulated but is much weaker than that in the Shindell et al. (1999) study. In the Geophysical Fluid Dynamics Laboratory warming experiments, which are of comparable resolution to the Fyfe et al. (1999) integrations, there is no AO trend (Kushner et al. 2001). By contrast, the response of the AAO to increasing CO_2 displays a robust definite upward trend in all transient greenhouse warming integrations.

Most of the warming experiments (e.g., Fyfe et al. 1999; Kushner et al. 2001) have the atmospheric equivalent CO_2 concentration that increases according to an

Corresponding author address: Dr. Wenju Cai, CSIRO Atmospheric Research, PMB 1, Aspendale, Vic 3195 Australia.
E-mail: wenju.cai@csiro.au

Intergovernmental Panel on Climate Change (IPCC) scenario (Houghton et al. 1992; Michell et al. 1995; Haywood et al. 1997). All scenarios include a transient period, in which the equivalent CO_2 increases at a specified rate from a reference level. So far, only the response of the AAO in the transient period has been studied. The subsequent behavior is yet to be explored. This is the major focus of the present study. We analyze the response of the atmospheric circulation simulated by the Commonwealth Scientific and Industrial Research Organisation (CSIRO) Mark 2 coupled GCM in three warming runs all following the IPCC IS92a scenario. During the transient period, the equivalent CO_2 increases from 1860 to 2083 when the CO_2 triples the level of the pre-1860 level. All three warming runs then include a stabilization period of several centuries in which the CO_2 is held at a constant, elevated $3 \times CO_2$ condition.

The rest of the paper is organized as follows. After describing the model and the experiments (section 2), we confirm the upward trend of the model AAO during the transient period and examine its subsequent behavior during the stabilization period, which shows a gradual reversal (section 3). We demonstrate that the response of the AAO is linked with that of the Southern Ocean (section 4), which is in turn associated with the feature of interhemispheric warming asymmetry (e.g., Stouffer et al. 1989).

2. Model and model experiments

The CSIRO Mark 2 coupled model (Gordon and O'Farrell 1997) has a horizontal resolution of the R21 spectral representation, or approximately 3.2° latitude $\times$ 5.6° longitude, in both the atmosphere and ocean submodels. The atmospheric general circulation model (GCM) has nine vertical sigma levels. It includes a semi-Lagrangian treatment of water vapor transport, dynamic sea ice, and a bare soil and canopy land surface, as well as standard parameterizations of radiation, cloud, precipitation, and the atmospheric boundary layer. The ocean GCM has 21 vertical levels, and includes the scheme of Gent and McWilliams (1990), which parameterizes the adiabatic transport effect of subgrid-scale eddies, and replaces the nonphysical horizontal diffusivity as a means of stabilizing the model numerics. The inclusion of the scheme results in a much improved stratification leading to a major reduction in convection at high southern latitudes. A detailed description of the improvements has been given by Hirst et al. (2000) and the improvement in the high-latitude Southern Ocean has also been discussed by Cai et al. (2001).

The model experiments comprise three control climate simulations [hereafter referred to as control 1 (Hirst et al. 2000), control 2 (Matear et al. 2000; Matear and Hirst 2002), and control 3 (Bi et al. 2001)] using three versions of the coupled model, each run for at least 600 yr of simulation. The three versions differ in terms of the ocean spinup strategy and ocean and sea ice parameterization. One difference lies in the forcing of the ocean spinup, in which the surface forcing fields have been modified such that the annual cycle of sea surface temperature (SST) and sea surface salinity over the deep water formation regions are increasingly better simulated from control 1 to control 3 (Bi et al. 2001). This results in a progressively stronger deep-penetrating North Atlantic deep water and more realistic water mass in the Southern Ocean from control 1 to control 3, yielding a stratification in control 3 that very closely matches the observed structure (see Bi et al. 2001 for further information). Another difference lies in the adjustment of the sea ice model (O'Farrell 1998), in which the sensitivity of sea ice to ocean heat exchange is made more realistic, increasing from control 1 to control 3 (S. O'Farrell 2002, personal communication). As a result, the sea ice amount in the control spinup state decreases from control 1 to control 3.

Transient greenhouse warming runs are then conducted using the three versions of the coupled model in which the model is forced by increasing levels of greenhouse gases as observed (1880–1990) and according to IPCC scenario IS92a (1990–2100; Houghton et al. 1992). The equivalent CO_2 concentration doubles at about year 2048 and triples at year 2083 from the pre-1880 level. Thus, in the model, the CO_2 evolution represents the changes of all anthropogenic greenhouse gases in the IS92a scenario. The three runs will be referred to as run 1 (Hirst 1999), run 2 (Matear et al. 2000; Matear and Hirst 2002), and run 3 (Bi et al. 2001), as they start from control 1, control 2, and control 3, respectively.

This period in which CO_2 increases is referred to as the transient period. Thereafter, each warming run is continued for another several hundred years under a constant $3 \times CO_2$ condition. This period is referred to as the stabilization period. At the time of analysis, the shortest run had been continued for about 400 yr under the $3 \times CO_2$ condition. We shall compare the response of the AAO in the three warming runs for the period that all three runs cover in common, that is, about 600 yr. Bi et al. (2001) described the response of the Southern Ocean overturning in run 3.

We apply empirical orthogonal function (EOF) analysis to outputs of annual-mean anomaly/change fields of Z500 to identify major modes in all three of the control and warming runs. We choose this variable because it is a commonly used field, thus facilitating comparison with results of other studies in terms of modes simulated in the control runs. For the three control runs, annual-mean anomalies are constructed from the long-term mean (averaged over a 600-yr period). For the three warming runs the changes are calculated with reference to the long-term mean of the respective control run.

In a recent study on projection of climate change onto modes of atmosphere variability, Stone et al. (2001) identified variability patterns in the control run, and then projected climate change signals onto these patterns. In

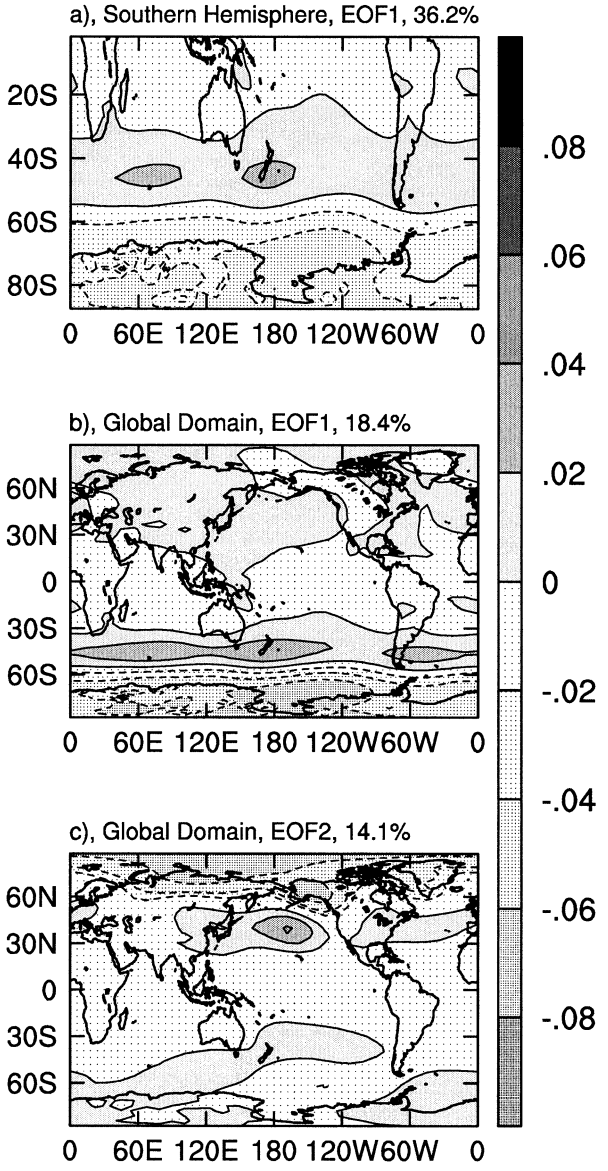

FIG. 1. (a) EOF1 of Z500 anomalies in the SH domain, and (b) EOF1 and (c) EOF2 of Z500 anomalies in the global domain, all from control 1.

the present studies, we follow the approach of Fyfe et al. (1999) and apply EOF analysis directly to the changes, allowing responses to manifest as modes that may be significantly different from those in the control run. If a mode from warming run outputs turns out to be the same as one from the respective control run outputs, it means that the response manifests as a preexisting mode in a natural way. In the event that a major response does not manifest as a preexisting mode, as is the case of the response of Z500 and SST, this approach provides an opportunity for such a response to be identified.

In one set of analyses, the domain is from the equator to the South Pole, and in another the domain is global. Throughout the study we use covariance matrix EOF analysis, and the gridpoint anomalies are neither area weighted nor normalized, as in other studies of SH variability (e.g., Kiladis and Mo 1999; Fyfe et al. 1999). While such an analysis approach gives a stronger emphasis on the high latitude, as variance there is greater than that at the low latitude in terms of Z500 or MSLP changes, it may be appropriate as we are interested in the AAO, which is mainly a mid- to high-latitude mode. To test the sensitivity to area weighting, we have conducted EOF analyses on area-weighted changes. We find that there is little change in terms of the order of modes or the percentage each accounts for.

Major modes of Z500 in the SH domain in control 2 have been recently examined by Cai and Watterson (2002). On interannual timescales, three modes are significant based on the North et al. (1982) criterion. The first mode is the AAO, which has also been referred to as the high-latitude mode (e.g., Mo and White 1985; Mo and Ghil 1987; Karoly 1990, 1995; Kidson and Sinclair 1995; Watterson 2000), or the zonally symmetric or annular mode (e.g., Kidson 1988), reflecting the feature of north–south out-of-phase variations between the Antarctic and midlatitudes at all longitudes. The spatial pattern from one of the runs is shown in Fig. 1a. The pattern correlation coefficients between the AAOs in the three control runs range between 0.97 and 0.99. In the three control runs, the second mode is the so-called Pacific–South American (PSA) pattern (Mo and Ghil 1987; Karoly 1989). The PSA is known to be strongly influenced by tropical convection, which generates wave trains extending across the South Pacific and South America (e.g., Berbery and Nogués-Paegle 1993; Kiladis and Weickmann 1997; Mo and Higgins 1997, 1998). In all three control runs, the third EOF is a mode with wavenumber-3 variability pattern in the latitude band of 40°–70°S (e.g., Mo and White 1985; Kiladis and Mo 1999; Cai et al. 1999). In this study, we focus mainly on the response of the AAO.

In all three control runs, EOF1 in the global domain is the AAO (the pattern for one of the runs is shown in Fig. 1b). These EOF1s account for approximately 18% of the total variance of each respective control run. The pattern correlation coefficients between any two AAO modes range between 0.97 and 0.98, and the pattern correlation coefficient (in the SH domain) between Figs. 1a and 1b reaches as high as 0.995. The correlation between the corresponding time series associated with Figs. 1a and 1b is virtually 1. In all three control runs, EOF2 in the global domain is the AO (the pattern for one of the runs is shown in Fig. 1c), each accounting for approximately 14% of the total variance in each respective control run. The pattern correlation coefficients between any two AO modes from the three control runs range between 0.88 and 0.91.

3. EOF of response in the warming runs

a. SH domain

In all three warming runs the first mode of Z500 changes shows an increase in height everywhere as the

coupled system warms up (Figs. 2a–c). The pattern correlation between any two patterns of Figs. 2a–c ranges between 0.98–0.99, highlighting the similar, systematic response in the three warming runs. These EOF1s account for 98.0%, 98.3%, and 97.9% of the total variance of runs 1, 2, 3, respectively. All three EOF1 patterns display a large increase over the Antarctic latitudes than over lower latitudes. This is associated with the so-called sea ice–albedo positive feedback: in the high and polar latitudes, the retreat of sea ice and/or snow greatly reduces surface albedo, leading to enhanced solar radiation to the surface and larger warming there. The evolution of the pattern (Fig. 2d) more or less follows that of the prescribed CO_2 increase. It features a steep upward trend as the model atmospheric CO_2 increases (during the transient period) and then a continued but moderate upward trend after the CO_2 concentration level is held constant (during the stabilization period). We will refer to this evolution as the ''upward and continued upward'' response or ''warming and continued warming'' response for the temperature field.

The warming trend shows significant differences from one run to another, and the differences are particularly prominent during the stabilization period; the warming is greater in run 3 than in run 2 and smallest in run 1. A primary factor is that from control 1 to control 3, the stratification of the Southern Ocean is progressively stronger. Thus, from run 1 to run 3, warming is pregressively more concentrated in the upper ocean. As a result, the upper-ocean warming rate is greatest in run 3, second in run 2, and smallest in run 1; in addition, sea ice reduction (in terms of percentage) is largest in run 3. Through sea ice–albedo positive feedback, the difference in sea ice response further enhances the difference of the warming rate in the three runs.

The second EOF in all three runs is an AAO-like (Figs. 3a–c) mode. They account for 0.9%, 0.8%, and 1.0% of the total variance of runs 1, 2, and 3, respectively. A statistical test using North et al's (1982) criterion reveals that although they account for a small percentage of the total variance, these EOF2s are statistically distinct from the EOF3s, which account for a maximum of 0.187% of the respective total variance. We have correlated each of the three patterns with the AAO pattern in the respective control run; the correlation coefficients range between 0.95 and 0.96, confirming that these modes are indeed the AAO. The systematic response of the coupled system is reflected by the high pattern correlation coefficients between any two patterns of Figs. 3a–c, which range between 0.98 and 0.99. The evolution shows an upward trend during the transient period, consistent with the findings of previous studies (e.g., Fyfe et al. 1999; Kushner et al. 2001). The central result here is the reversal and gradual recovery during the stabilization period to the level prior to the CO_2 forcing. The time needed for the recovery appears to be different from one run to another, again dependent upon the initial coupled climate state and the parameters

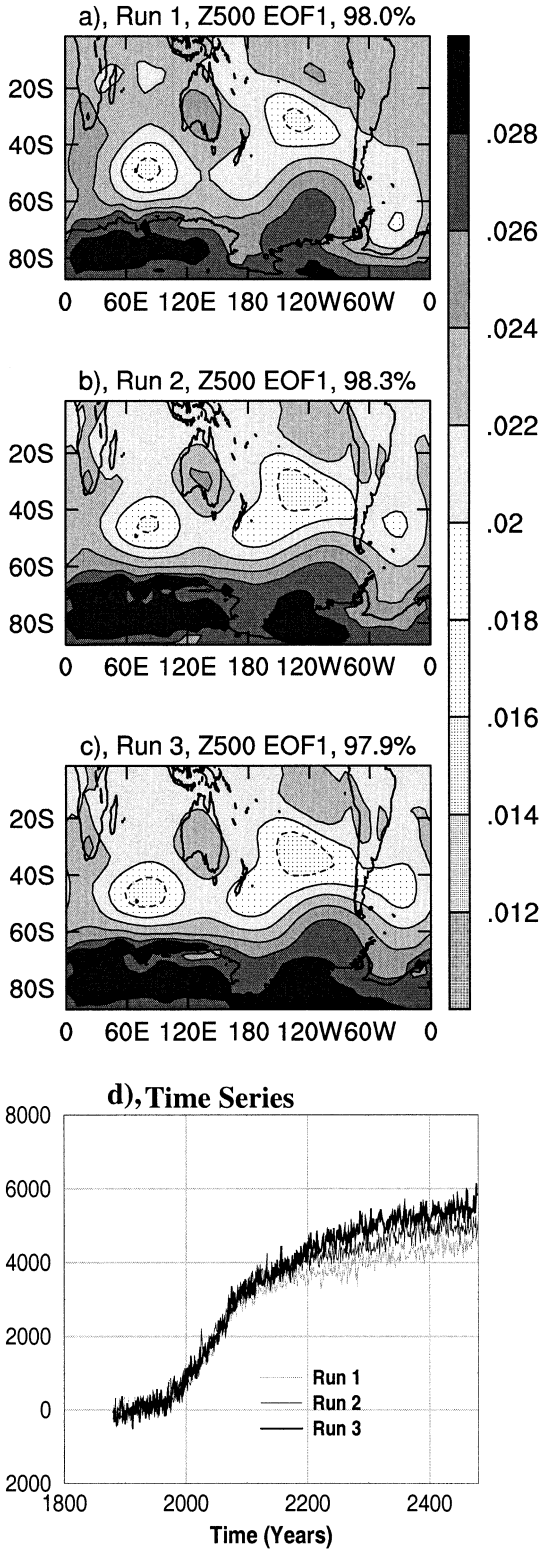

FIG. 2. EOF1 of Z500 changes from (a), (b), (c) the three warming runs and (d) their corresponding time series. The pattern is not a predominant mode in its corresponding control run.

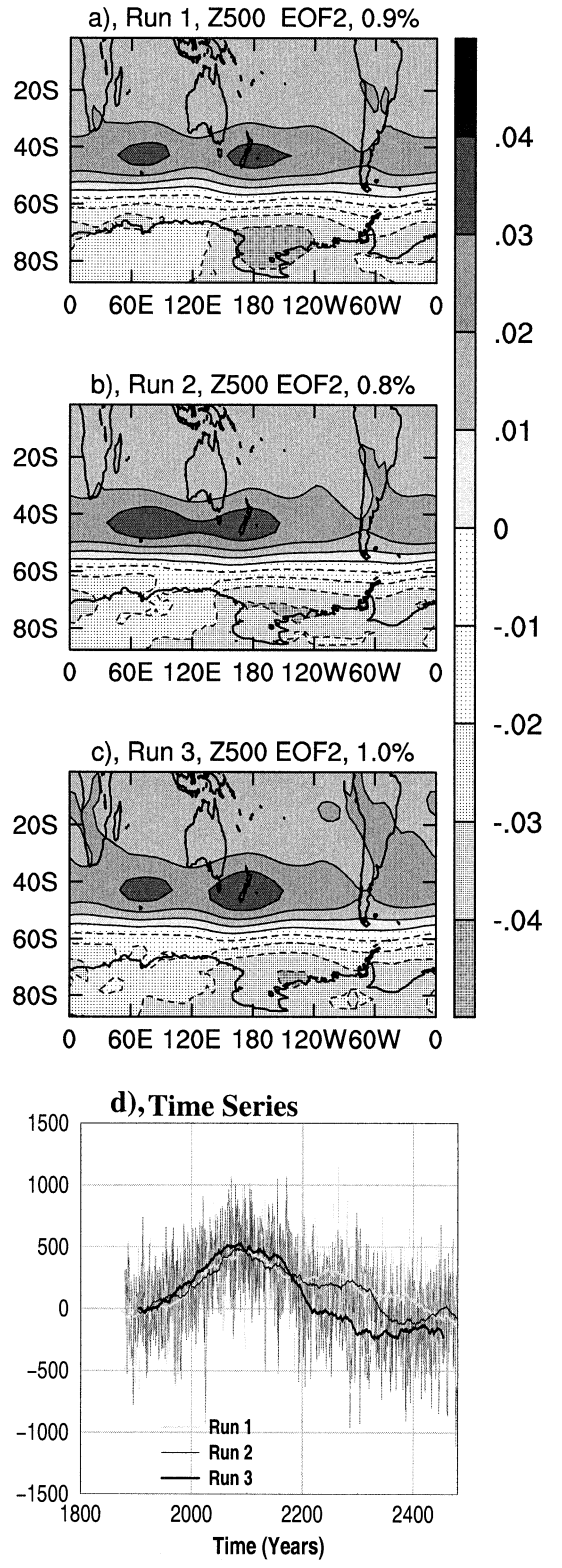

FIG. 3. EOF2 of Z500 changes from (a), (b), (c) the three warming runs and (d) their corresponding time series. The 51-yr running mean version of and the raw EOF time series are shown in (d). The pattern is similar to that of the EOF1 of Z500 in the SH domain in its respective control run.

of the coupled system. We will refer to this evolution as the ''trend-reversing'' response. The reversal of the AAO is also confirmed by linear trend maps of Z500 fields for the two subperiods before and after year 2083, both being similar to the patterns of Figs. 3a–c.

The pattern of Z500 EOF1 also shows some meridional gradients in the southern midlatitudes. This raises a question as to whether the AAO response also projects onto the Z500 EOF1. To address this issue, we have regressed, year by year, the Z500 change fields of a warming run onto the AAO pattern of each respective control run. This yields a time series of regression coefficients for each run nearly identical to the time series of EOF2 in the respective warming run. This result suggests that little of the AAO response projects onto the Z500 EOF1. As will be clear, the forcing of the two Z500 EOFs is quite different.

Some comments on the large difference in the variance explained by Z500 EOF1 and EOF2 are in order. The large difference means that in terms of Z500 changes, EOF1 is by far the largest response. In the Fyfe et al. (1999) study, in which they applied EOF analysis on MSLP response, none of their EOF patterns show as strong a direct greenhouse warming–related signal as the Z500 EOF1 presented here. In our warming runs, EOF1 of the MSLP changes is also AAO-like (Figs. 4a–c), with a pattern similar to that of the Z500 EOF2 changes, and accounts for about 45% of the total variance, consistent with the results of Fyfe et al. (1999). Thus, although the AAO-like response in Z500 appears to be small (about 1% the total change as described above), at the surface it is the principal response pattern. The evolution (Fig. 4d) is also similar to that of Z500 EOF2, with the trend-reversing feature. The second EOF of the MSLP (not shown), which corresponds to the Z500 EOF1, accounts for about 16% of the total variances and the evolution shows an upward and continued upward response. The fact that Z500 EOF1 show a stronger warming signal than the MSLP EOF1 may indicate that MSLP EOF1 reflects a barotropic component of the response, whereas the Z500 EOF1 represents a baroclinic component of the response with a strong thermal change in the lower troposphere.

The above results suggest that while the response can manifest as a mode that is preexisting in the control run (Stone et al. 2001) the system can also generate a mode of response that is not preexisting. More importantly, the response that projects onto the preexisting mode has a trend that exists only temporarily, and in the present case reverses once the CO_2 concentration stabilizes, highlighting the importance of achieving a stabilization of the atmospheric CO_2 concentration.

To examine the coherence of changes of Z500 with those of temperature, an EOF analysis on SST and/or surface temperature changes has been conducted. We find that the above two modes of Z500 have corresponding modes in SST and surface temperature changes. The patterns of SST EOF1 in the three warming runs

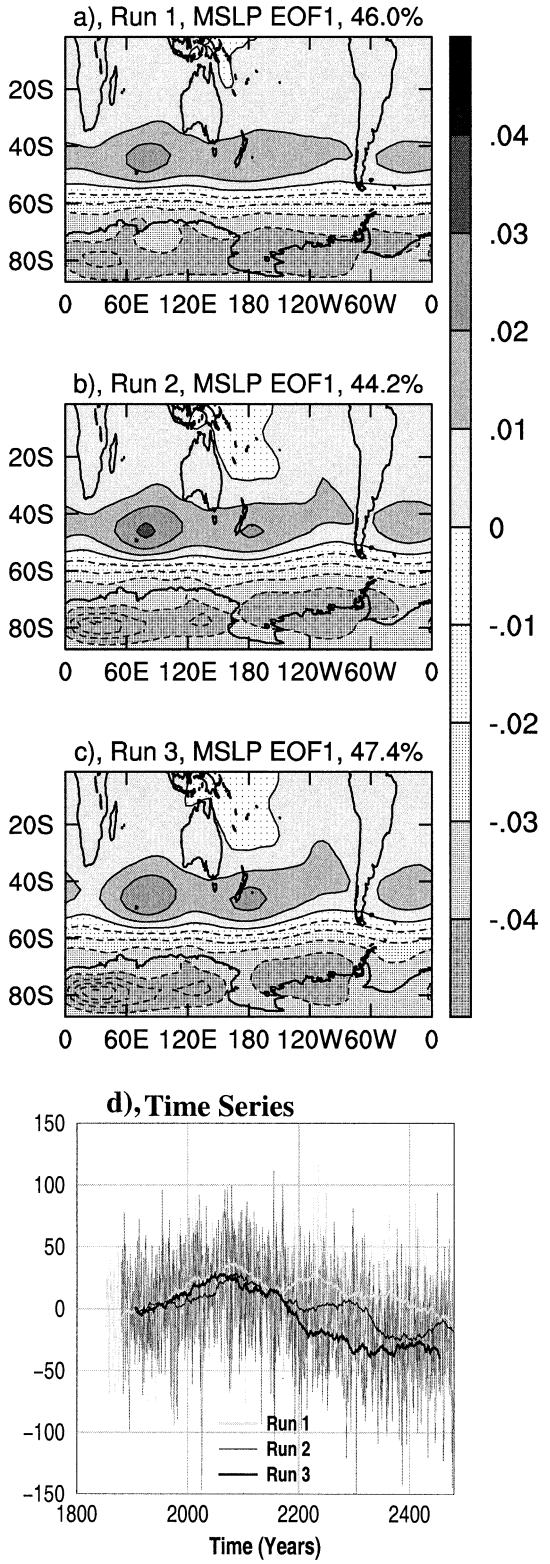

FIG. 4. EOF1 and MSLP changes from (a), (b), (c) the three warming runs and (d) their corresponding time series. The 51-yr running mean version of and the raw EOF time series are shown in (d). The pattern is similar to that of the EOF1 of MSLP in the SH domain in its respective control run.

(Figs. 5a–c) show that warming takes place everywhere, with a greater rate over high and polar latitudes (particularly over sea ice regions) than over the low and midlatitudes. We will refer to this mode as the polar amplification mode. The EOF1 of surface temperatures shows a similar pattern, with generally larger warming over land than over the oceans. The large warming in the polar and high latitudes is a direct effect of the polar amplification, as described above. That such a response is systematic is evident in the resemblance among Figs. 5a–c. The correlation coefficients between any two patterns of Figs. 5a–c that are in the range of 0.98–0.99. The temporal evolution again shows a warming and continued warming trend. In the stabilization period, there are noticeable differences among the three runs, similar to that of the Z500 EOF1 (see Fig. 2d): the rate of warming is greatest in run 3, second in run 2, and lowest in run 1.

The patterns of the SST EOF2 (Figs. 6a–c) show weights of opposite polarity north and south of about 45°S, with maximum negative weights in the areas of the Ross and Weddell Seas. The pattern correlation coefficients among them are again high, in the range of 0.91–0.95. The patterns together with the temporal evolution (Fig. 6d) indicate that during the transient period, the warming rate decreases poleward; and there is a relative cooling trend in the latitudes south of approximately 45°S. This is strongest in the convection regions. By ''relative'' we mean that the cooling trend takes place simultaneously with the polar amplification warming mode (EOF1), which shows a general warming trend. On balance, there is net warming. In other words, the cooling trend applies only after the warming trend associated with EOF1 has been removed. For this reason we will interpret the EOF2 pattern as one with slower warming in the high latitudes than at lower latitudes, and the associated time series during the transient period as a ''relative cooling trend,'' that is, relative to the general warming trend associated with the polar amplification mode.

There are several reasons for this spatial distribution of the SST EOF2. First, as noted in previous studies (Stouffer et al. 1989; Bryan et al. 1988), warming in the SH is smaller than in the NH because of the higher fraction of area covered by the ocean, which has a higher thermal inertia, highest along the latitude band of about 45°–65°S, as it is completely covered by ocean. In section 3b, we will show that this EOF2 pattern is part of the interhemispheric asymmetry warming response proposed by Bryan et al. (1988) and Stouffer et al. (1989). Second, off the Antarctic coast, as sea ice melts, the SST is ''regulated'' by the freezing temperature, also making it difficult to warm. In such a background, it is the weakening of the convective mixing, whereby less and less warm subsurface water is brought to the surface, that is responsible for the strong relative cooling trend. As will be discussed in section 4, feedbacks between atmospheric fields of surface pressure, albedo, and surface temperature

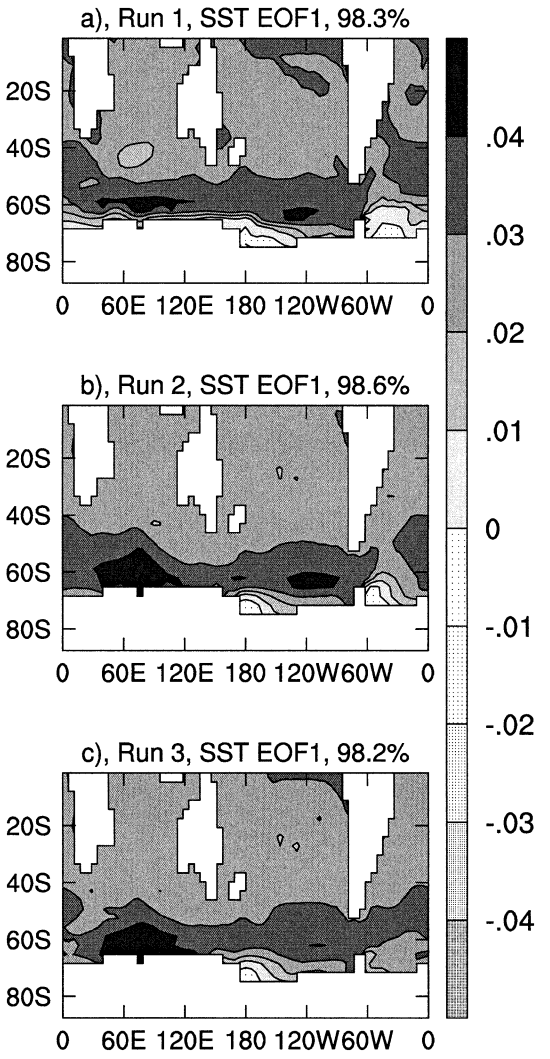

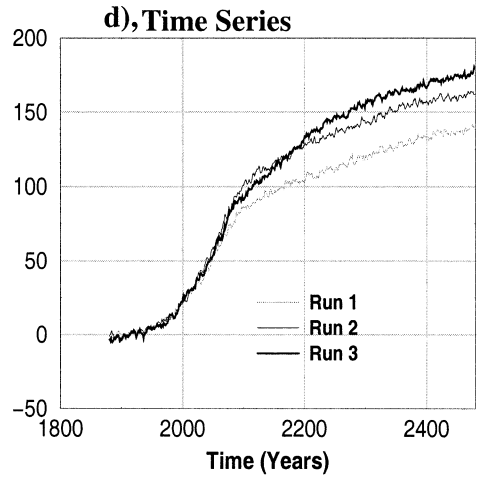

FIG. 5. EOF1 of SST changes from (a), (b), (c) the three warming runs and (d) their corresponding time series. The pattern is not a predominant mode in its respective control run.

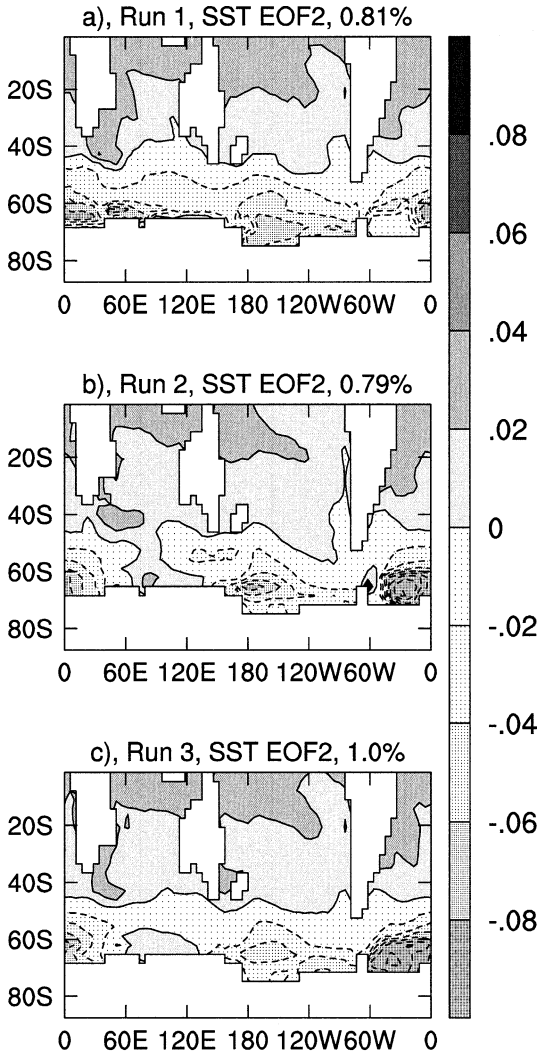

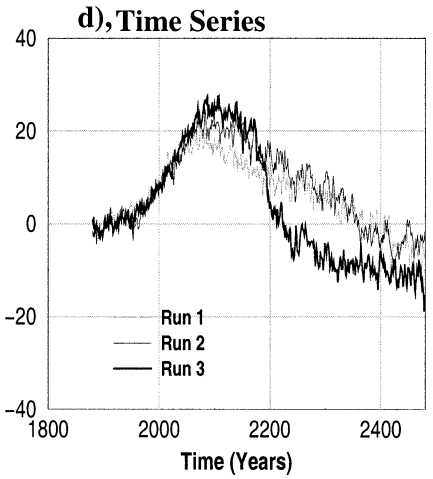

FIG. 6. EOF2 of SST changes from (a), (b), (c) the three warming runs and (d) their corresponding time series.

tend to reinforce the pattern. During the stabilization period it is this relative cooling that reverses, as the high-latitude ocean warming catches up.

Apparently, the polar amplification mode does not have a corresponding mode in the control run. To examine whether the SST EOF2 in the warming run has one, we have applied EOF analysis on the control run SST anomalies in the SH domain. The first three modes are similar to those described in Cai and Watterson (2002). The first EOF is an El Niño–like mode and accounts for about 11.8% of the total variance; the second EOF is most similar to those shown in Figs. 6a–c, and accounts for about 6.8% of the total variance; and the third EOF is the wavenumber-3 pattern (Cai et al. 1999). Nevertheless, the pattern correlation coefficients between the SST EOF2 in the warming runs and the SST EOF2 in the control runs are small, in the range of 0.32–0.34. This result suggests that most of the SST response does not project into the preexisting modes of the control runs.

b. Global domain

Is the response obtained in the SH domain part of the global response? To address this issue, we apply EOF analysis in the global domain. The global Z500 EOF1s account for 98.2%, 98.3%, and 98.3% of the total variance for run 1, run 2, and run 3, respectively. The weight distribution in the SH of global Z500 EOF1 is similar to the SH Z500 EOF1, both showing increased heights everywhere, but with a greater increase over the polar latitudes and land areas (Figs. 7a–c) than over the ocean. The time evolution (Fig. 7d) displays the familiar upward and continued upward evolution. The global Z500 EOF2 (Figs. 8a–c) is the AAO mode; each of the patterns is highly correlated with that of the global EOF1 of the respective control run (correlation coefficients in the range of 0.93–0.97). The response is again systematic, all showing the trend-reversing response. Overall, these results suggest that the response obtained in the SH domain is part of the global changes.

The first mode of surface temperature (Figs. 9a–d) in the global domain highlights the fact that the systematic response with the polar amplification of warming takes place in both hemispheres. The global EOF2 of surface temperature (Figs. 10a–d) is equivalent to the SH SST (or surface temperature) EOF2: in southern mid- to high latitudes there is an initial relative cooling (strongest in high-latitude convection regions) during the transient period and an acceleration of warming during the stabilization period. The latitudinal warming difference seen in Fig. 6 is clearly embedded in this mode. This is the interhemispheric mode discussed by Bryan et al. (1988) and Stouffer et al. (1989), which reflects the delay in warming in the SH already discussed in section 3a. The interhemispheric asymmetry in an early version of the CSIRO coupled GCM has been described by Cai and Gordon (1998).

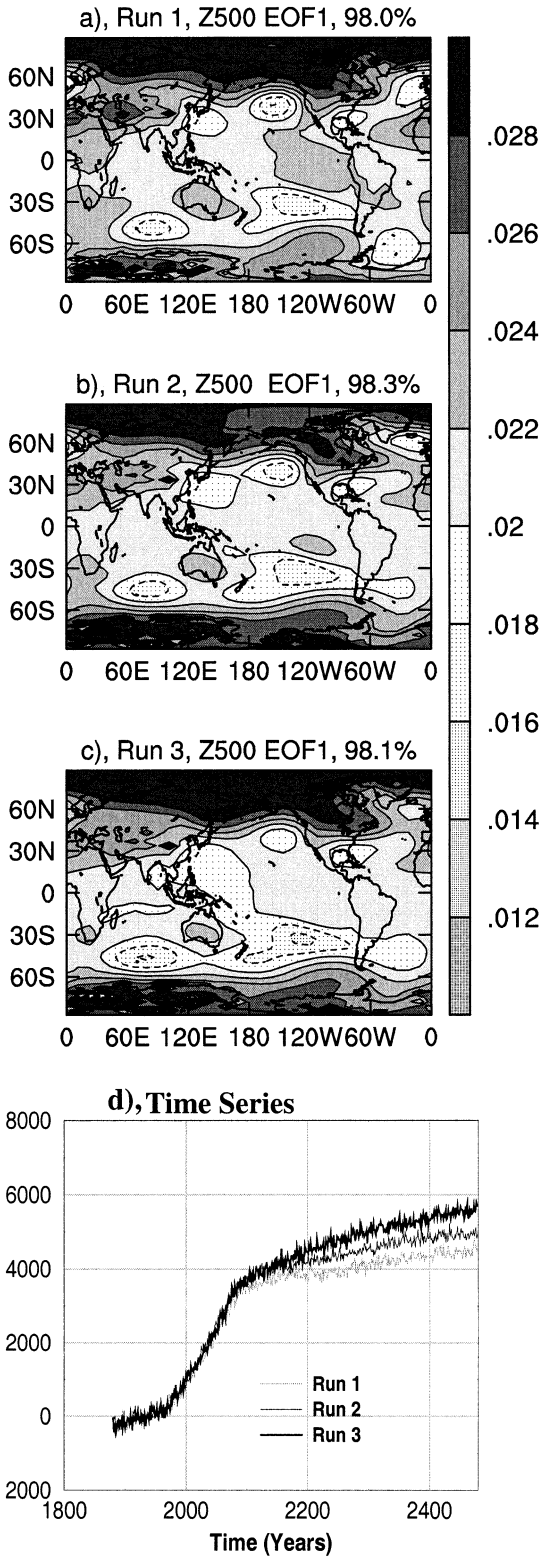

FIG. 7. EOF1 of Z500 changes from (a), (b), (c) the three warming runs and (d) their corresponding time series. The pattern is not a predominant mode in its respective control run.

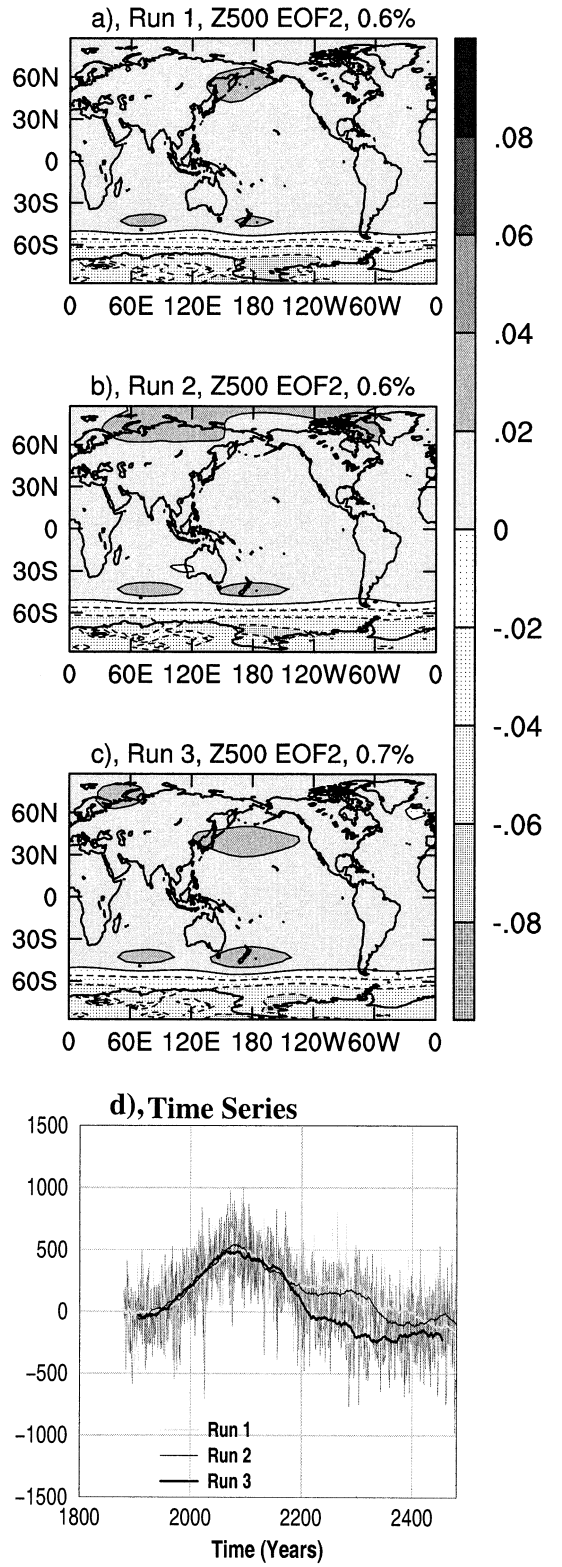

FIG. 8. EOF2 of Z500 changes from (a), (b), (c) the three warming runs and (d) their corresponding time series. The 51-yr running mean version of and the raw EOF time series are shown in (d). The pattern is similar to a dominant mode (EOF1) in its respective control run.

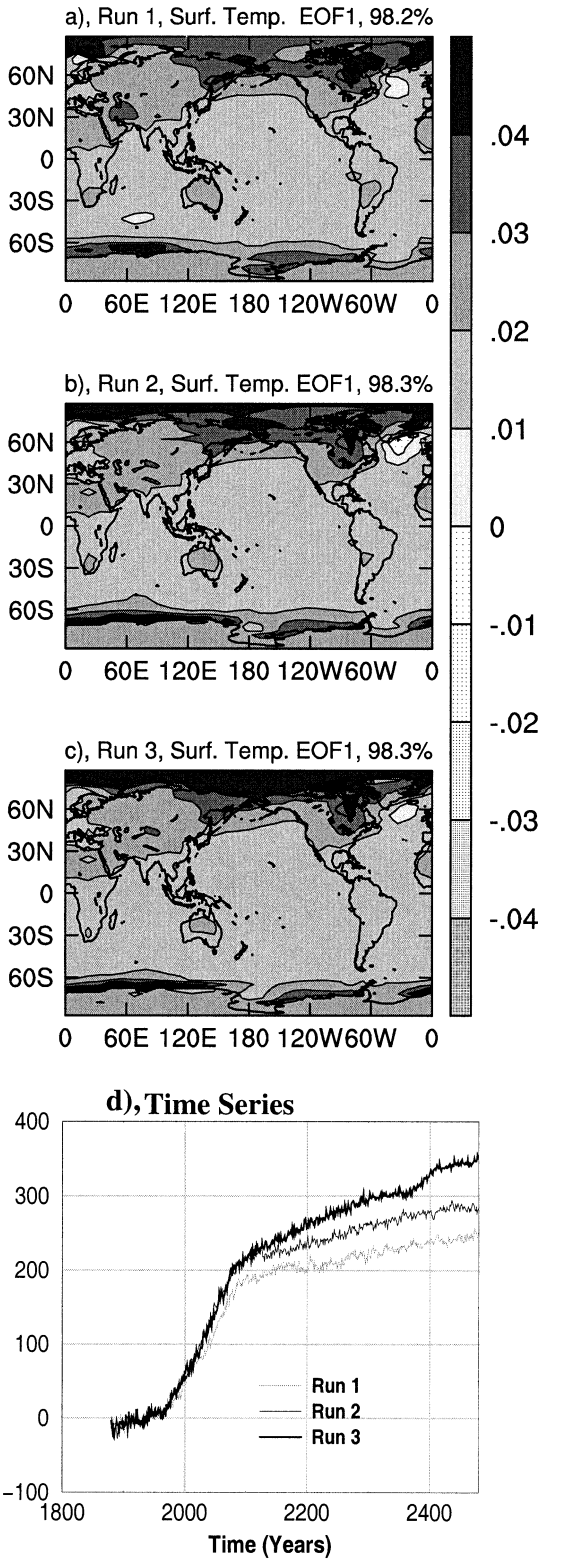

FIG. 9. EOF1 of SST changes from (a), (b), (c) the three warming runs and (d) their corresponding time series. The pattern is not a predominant mode in its respective control run.

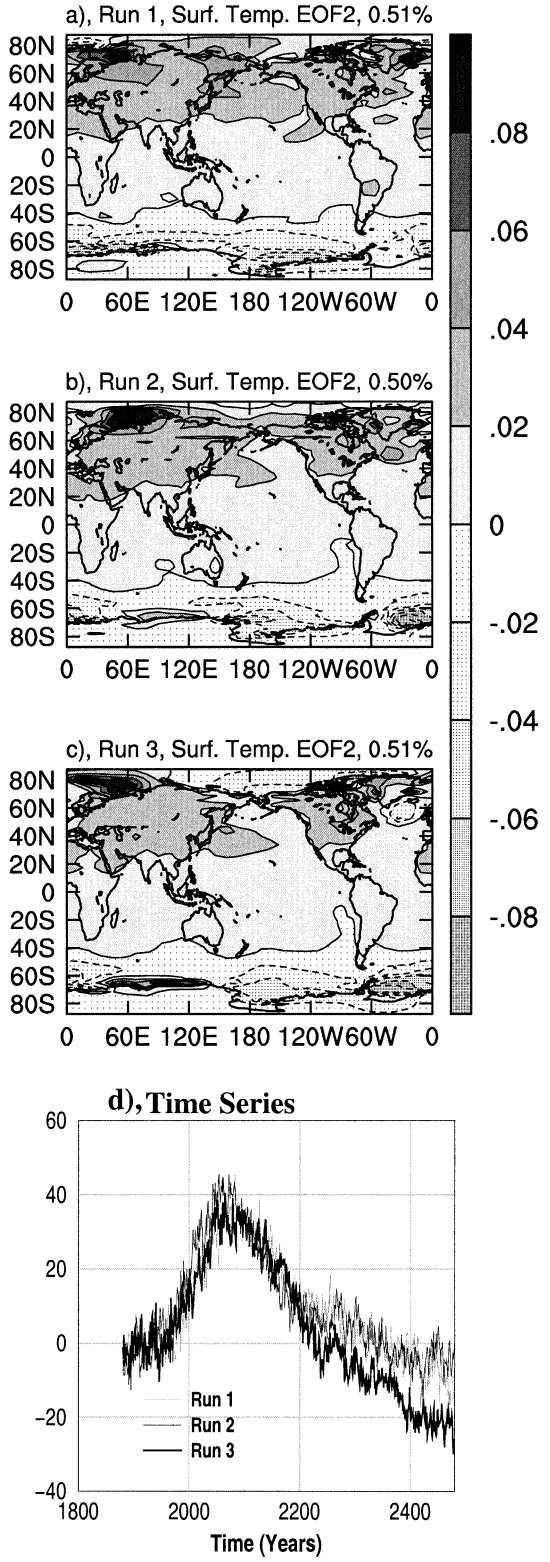

FIG. 10. EOF2 of SST changes from (a), (b), (c) the three warming runs and (d) their corresponding time series. The pattern is not a dominant mode in its respective control run.

Examinations reveal that there is no interhemispheric mode of SST (or surface temperature) anomalies in the control runs. Thus, the major response, in both EOF1 and EOF2, of SST (or surface temperature) does not project onto a preexisting mode. In analyses of changes during the twentieth century, Cai and Whetton (2000, 2001) found that in the tropical Pacific, the response pattern of SST changes in ENSO–like. In the present analysis, the ENSO variability-like response appears as EOF3.

4. Discussion

a. The response of the AO

So far, we have not discussed the response of the AO. The EOF analysis of Z500 anomalies in the NH domain shows that the AO is the most dominant mode in all three control runs. As discussed in section 2, the AO is also the second most dominant mode in the global domain. In the three warming runs, the global Z500 EOF3 (Fig. 1c) is the AO mode (Figs. 11a–c). The pattern correlation coefficients between this mode in the warming run and the corresponding mode (Fig. 1c) in the respective control run are in the range of 0.88–0.91. However, the time series (Fig. 11d) shows that there is little trend in the warming runs. It is not clear whether or not the lack of an AO trend is due to model resolution in the stratosphere. The main conclusion we arrive at is that in our model, besides the mode of the upward and continued upward trend response, the remaining change in Z500 projects mainly onto the AAO.

b. The dynamic environment for the AAO evolution

The trend-reversing evolution of both the AAO and the temperature interhemispheric asymmetry mode suggest that the dynamics for these responses are linked. On the basis that only the ocean has a memory of timescales of several centuries, we suggest that the trend-reversing evolution of the AAO (Z500 EOF2) is dynamically determined by the temperature interhemispheric asymmetry mode. In the following we discuss the relationship between the AAO and temperature in the control runs, and then comment on the dynamics that support this relationship in the warming runs.

The relationship between the AAO and surface temperature in control 2 (the respective control run of run 2) has been recently examined by Cai and Watterson (2002). They showed that the temperature anomaly pattern associated with the AAO displays zonally symmetric anomalies of opposing signs in the meridional direction (see their Fig. 3a). Over the latitudes where height (and MSLP) anomalies are positive, cloud cover decreases, leading to an increased incoming radiative heat flux and, hence, anomalously warm surface temperatures. Over the latitudes with negative height anomalies: total cloud cover increases and less energy pen-

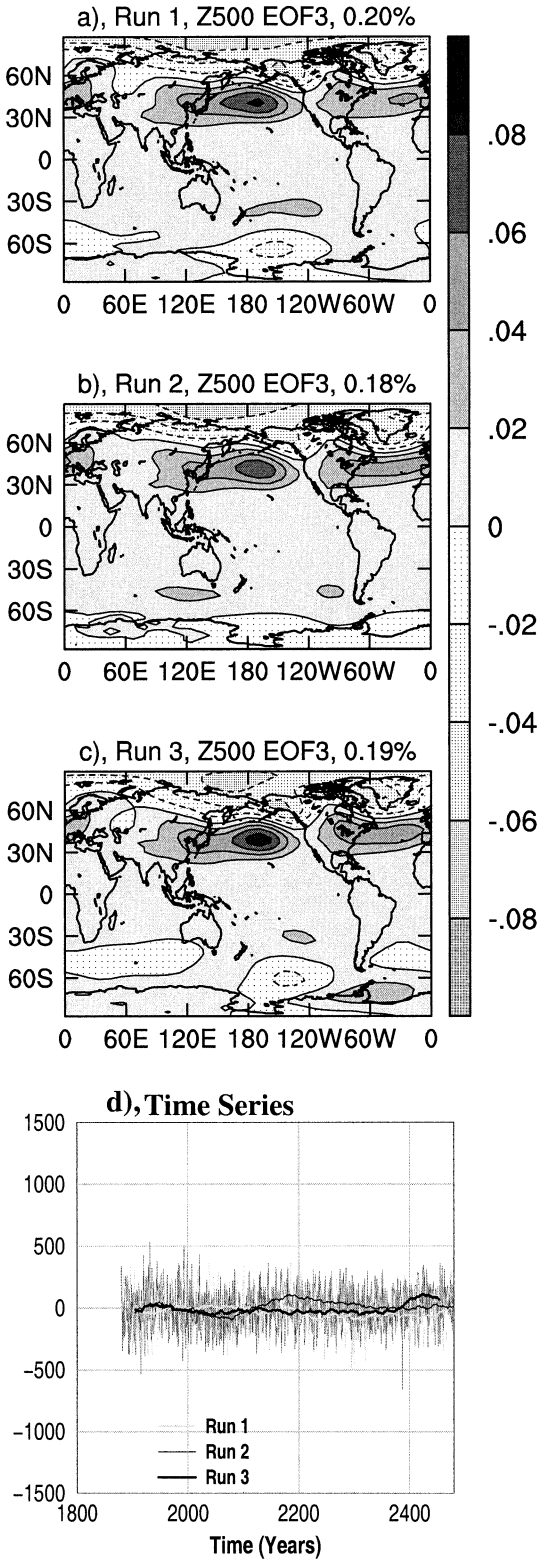

FIG. 11. EOF3 of Z500 changes from (a), (b), (c) the three warming runs and (d) their corresponding time series. The 51-yr running mean version of and the raw EOF time series are shown in (d). The pattern is similar to a dominant mode (EOF2) in its respective control run.

etrates to the surface, leading to the development of negative surface temperature anomalies. This relationship exists in all three control runs.

The association of negative temperature weights with negative height weights in the polar latitudes, and vice versa in the mid- to high latitudes (Figs. 3a–c and 6a–c), is therefore a continuation of the relationship that exists in the control runs. During the transient period, decreasing MSLP over the relative cooling region (approximately 45°S poleward) provides favorable conditions for clouds and rainfall to increase. By contrast, north of the oceanic convective regions, the reverse is true: cloud cover and rainfall decreases (the rainfall response will be discussed further in section 4c). This latitudinal setting reverses during the stabilization period in which warming in the Southern Ocean catches up with a greater warming rate in the higher latitudes than in the lower latitudes. This situation provides an appropriate dynamical environment in which the AAO reverses its trend and follows the evolution of the temperature EOF2.

The trend-reversing response of surface temperature, as manifested in Z500 EOF2, is not surprising given the well-known response of interhemispheric warming asymmetry. Indeed it is reassuring that such a feature manifests as an EOF mode. The central result here is that it shows a clear linkage to the AAO. The associated trend-reversing evolution implies that if CO_2 stabilization is achieved, the trend of the AAO established during the transient period is likely to reverse. This is because the latitudinal warming differences of the Southern Ocean will eventually be eliminated.

c. Implications of the AAO evolution for climate impacts

To discuss the issue of possible climate impacts of the model AAO response, it is appropriate to comment on the behavior of the observed AAO over the past decades and its possible linkage with other climate variables. Figures 12a and b show the AAO trend and pattern from an EOF analysis of monthly MSLP anomalies from 1957 onward of the National Centers for Environmental Prediction (NCEP) reanalysis. A general upward trend is seen, as noted by previous studies. The trend is particularly steep in the late 1960s. This coincides with a significant decrease in rainfall over southwest part of western Australia (SWWA; 120°E westward and 132°S southward; Smith et al. 2000). There is vigorous debate as to whether or not, and to what extent, the observed drying trend is induced by greenhouse warming.

The upward trend of the AAO means that the MSLP in the midlatitudes strengthens (Fig. 12b), providing a large-scale condition for the decreasing rainfall. Figure 12c depicts a map of correlation coefficients between the time series of the AAO mode (Fig. 12a) and NCEP monthly rainfall anomaly fields. It shows that when the

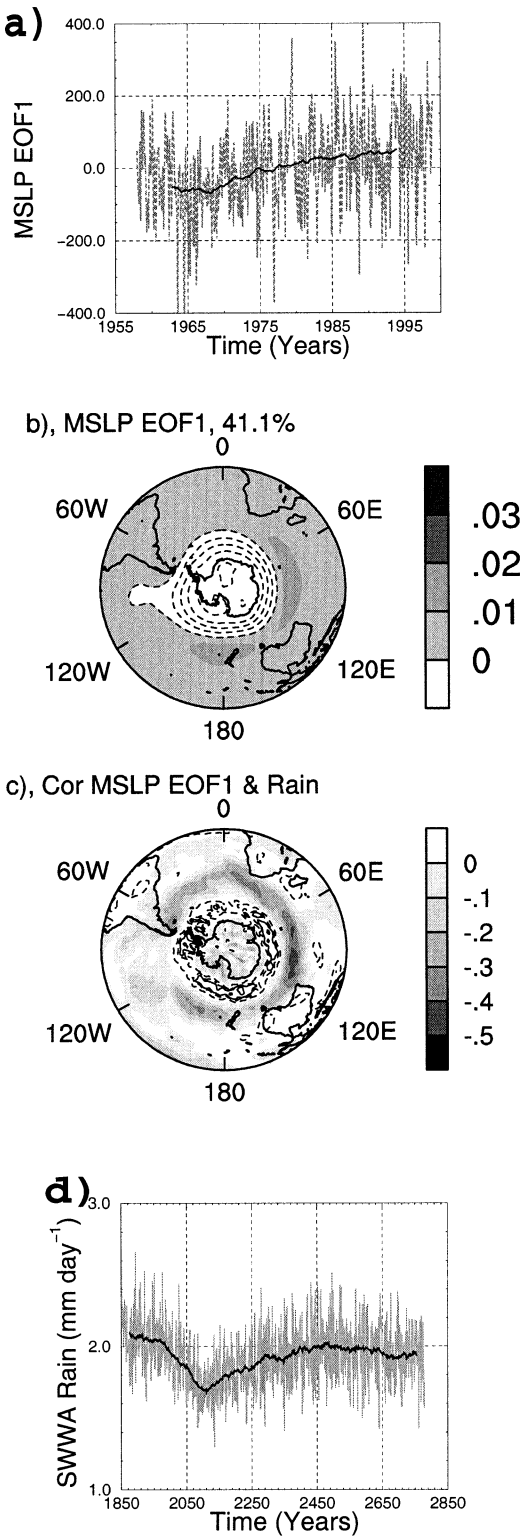

FIG. 12. (a) Time series and (b) pattern of EOF1 of monthly MSLP anomalies from NCEP reanalysis from 1957 onward. In (a), a 10-yr running mean curve is superimposed. (c) Map of correlation coefficients between the MSLP EOF1 time series and monthly rainfall anomalies. The contour interval is 0.1. (d) Time series of annual-mean rainfall over SWWA from a greenhouse warming run forced by the IPCC IS92a scenario in which the atmospheric CO_2 triples the initial value by year 2083 and is thereafter held at the elevated $3 \times CO_2$ level; a 51-yr running mean curve is also displayed in the plot.

AAO is positive there is indeed a tendency for rainfall over SWWA to decrease. The implication is that if the observed upward trend of the AAO is driven by greenhouse warming, it is likely that some of the drying trend is greenhouse induced as well.

Cai and Watterson (2002) showed that in the control runs the above relationship between the AAO and rainfall over SWWA is realistically simulated: when the AAO is positive, that is, with increased heights and MSLP in the midlatitudes, rainfall over SWWA tends to decrease as a result of decreased westerly winds, bringing less frontal events to SWWA.

Figure 12d shows a time series of rainfall change over SWWA in one of the warming runs. Rainfall over SWWA experiences a decreasing trend during the transient period, consistent with the observed decrease over the past several decades, thus, supporting the argument that the observed drying trend may be partially induced by global warming. In the stabilization period, rainfall there undegoes a gradual recovery, taking some 500 yr to do so. The course of evolution is robust and is seen in all three warming runs.

It follows that climate impacts associated with the AAO trend established in the transient period may be reversible if CO_2 stabilization is achieved. Whetton et al. (1997) applied EOF analysis to rainfall changes in run 1. The EOFs 1 and 2 display the familiar upward and continued upward and trend-reversing evolution, respectively. In many places, where rainfall responses is predominantly controlled by EOF2, the trend established during the transient period reverses. The modeled rainfall response over SWWA, as shown in Fig. 12d, is one excellent example, and it highlights the importance of achieving CO_2 stabilization.

5. Conclusions

Recent studies have consistently shown that under increasing atmospheric CO_2 concentration, the AAO displays an upward trend. However, its response during a subsequent CO_2 stabilization period has not been examined. In the present study, we show that the upward trend of the AAO reverses during such a stabilization period. This course of evolution is present in all three members of the ensemble. The evolution is determined by the latitudinal temperature gradients across the southern mid- to high latitudes embedded in the well-known interhemispheric warming asymmetry mode identified by previous studies. The fact that latitudinal warming differences will eventually be eliminated once CO_2 stabilization is achieved could therefore underpin the ro-

bustness of the AAO reversal. One important implication of our result is that climatic impacts of greenhouse warming associated with the AAO trend during the transient period may be reversible if CO_2 stabilization is achieved. The above conclusions are based on the assumption that any AAO trend is forced by greenhouse warming alone. Therefore, these conclusions may not be true in a situation in which the AAO trend is also driven by other forcings, as may to be the case over the past several decades (Thompson and Solomon 2002).

Acknowledgments. This work was supported by the Australian Greenhouse Office. We gratefully acknowledge the efforts of members of the Climate Modeling Program and the Atmospheric Processes Program at CSIRO Atmospheric Research in developing the model used in this study. We thank Paul J. Kushner and an anonymous reviwer for their helpful and insightful comments. We are grateful to Anthony Hirst and Dave Bi for permission to use their model outputs, and Prof. Bill Budd for providing the computational resources to support several of their integrations. Thanks also to Debbie Abbs and Anthony Hirst for reviewing our manuscript before submission.

REFERENCES

Berbery, E. H., and J. Nogués-Paegle, 1993: Intraseasonal fluctuations between the Tropics and extratropics in the Southern Hemisphere. *J. Atmos. Sci.,* **50,** 1950–1965.

Bi, D., W. F. Budd, A. C. Hirst, and X. Wu, 2001: Collapse and reorganization of the Southern Ocean overturning under global warming in a coupled model. *Geophys. Res. Lett.,* **28,** 3927–3930.

Bryan, K., S. Manabe, and M. J. Spelman, 1988: Interhemispheric asymmetry in the transient response of a coupled ocean–atmosphere model to a CO_2 forcing. *J. Phys. Oceanogr.,* **18,** 851–867.

Cai, W., and H. B. Gordon, 1998: Transient responses of the CSIRO climate model to two different rates of CO_2 increase. *Climate Dyn.,* **14,** 503–516.

——, and P. H. Whetton, 2000: Evidence for a time-varying pattern of greenhouse warming in the Pacific Ocean. *Geophys. Res. Lett.,* **27,** 2577–2580.

——, and ——, 2001: Time-varying greenhouse warming pattern and the tropical–extratropical circulation linkage in the Pacific Ocean. *J. Climate,* **14,** 3337–3355.

——, and I. G. Watterson, 2002: Modes of interannual variability of the Southern Hemisphere circulation simulated by the CSIRO climate model. *J. Climate,* **15,** 1159–1174.

——, P. G. Baines, and H. B. Gordon, 1999: Southern mid- to high-latitude variability, a zonal wavenumber-3 pattern, and the Antarctic Circumpolar Wave in the CSIRO coupled model. *J. Climate,* **12,** 3087–3104.

——, ——, and ——, 2001: Reply. *J. Climate,* **14,** 1332–1334.

Fyfe, J. C., G. J. Boer, and G. M. Flato, 1999: The Arctic and Antarctic Oscillations and their projected changes under global warming. *Geophys. Res. Lett.,* **26,** 1601–1604.

Gent, P. R., and J. C. McWilliams, 1990: Isopycnal mixing in ocean circulation models. *J. Phys. Oceanogr.,* **20,** 150–155.

Gordon, H. B., and S. P. O'Farrell, 1997: Transient climate change in the CSIRO coupled model with dynamic sea ice. *Mon. Wea. Rev.,* **125,** 875–907.

Haywood, J., R. Stouffer, R. Wetherald, S. Manabe, and V. Ramaswamy, 1997: Transient response of a coupled model to estimated changes in greenhouse gas and sulfate concentrations. *Geophys. Res. Lett.,* **24,** 1335–1338.

Hirst, A. C., 1999: The Southern Ocean response to global warming in the CSIRO coupled ocean–atmosphere model. *Environ. Model. Software,* **14,** 227–242.

——, S. P. O'Farrell, and H. B. Gordon, 2000: Comparison of a coupled ocean–atmosphere model with and without oceanic eddy-induced advection. Part I: Ocean spinup and control integrations. *J. Climate,* **13,** 139–163.

Houghton, J. T., B. A. Callander, and S. K. V. Varney, Eds.,1992: *Climate Change 1992—The Supplementary Report to the IPCC Scientific Assessment.* Cambridge University Press, 200 pp.

Hurrell, J. W., 1995: Decadal trend in the North Atlantic Oscillation: Regional temperature and precipitation. *Science,* **269,** 676–679.

Karoly, D., 1989: Southern Hemisphere circulation features associated with El Niño–Southern Oscillation events. *J. Climate,* **2,** 1239–1252.

——, 1990: The role of transient eddies in low-frequency zonal variations of the Southern Hemisphere circulation. *Tellus,* **42,** 41–50.

——, 1995: Observed variability of the Southern Hemisphere atmospheric circulation. *Natural Climate Variability on Decade-to-Century Time Scales*, National Academy Press, 111–118.

Kidson, J. W., 1988: Indices of the Southern Hemisphere zonal wind. *J. Climate,* **1,** 183–194.

——, and M. R. Sinclair, 1995: The influence of persistent anomalies on Southern Hemisphere storm tracks. *J. Climate,* **8,** 1938–1950.

Kiladis, G. N., and K. M. Weickmann, 1997: Horizontal structure and seasonality of large-scale circulation associated with submonthly tropical convection. *Mon. Wea. Rev.,* **125,** 1997–2013.

——, and K. C. Mo, 1999: Interannual and intraseasonal variability in the Southern Hemisphere. *Meteorology of the Southern Hemisphere, Meteor. Monogr.,* No. 35, Amer. Meteor. Soc., 307–336.

Kushner, P. J., I. M. Held, and T. L. Delworth, 2001: Southern Hemisphere atmospheric circulation response to global warming. *J. Climate,* **14,** 2238–2249.

Matear, R., A. C. Hirst, 2002: Long term changes in dissolved oxygen concentrations in the ocean caused by protracted global warming. *Geochem. Geophys. Geosyst.,* in press.

——, ——, and B. I. McNeil, 2000: Changes in dissolved oxygen in the Southern Ocean with climate change. *Geochem. Geophys. Geosyst.,* **1,** 2000GC00086. [Available online at http://www.g-cubed.org/.]

Michell, J., T. Johns, J. Gregory, and S. Tett, 1995: Climate response to increasing levels of greenhouse gases and sulphate aerosols. *Nature,* **376,** 501–504.

Mo, K. C., and C. H. White, 1985: Teleconnections in the Southern Hemisphere. *Mon. Wea. Rev.,* **113,** 22–37.

——, and M. Ghil, 1987: Statistics and dynamics of persistent anomalies. *J. Atmos. Sci.,* **44,** 877–901.

——, and R. W. Higgins, 1997: Planetary waves in the Southern Hemisphere and linkages to the tropics. Harry van Loon Symposium, Studies in Climate, Part II. NCAR Tech. Note TN-433+Proc., 290 pp.

——, and ——, 1998: The Pacific–South American modes and the tropical convection during the Southern Hemisphere winter. *Mon. Wea. Rev.,* **126,** 1581–1596.

North, G. N., T. L. Bell, R. F. Cahalan, and F. J. Moeng, 1982: Sampling error in the estimation of empirical orthogonal functions. *Mon. Wea. Rev.,* **110,** 699–706.

O'Farrell, S. P., 1998: Sensitivity study of a dynamical sea ice model: The effect of the external stresses and land boundary conditions on ice thickness distribution. *J. Geophys. Res.,* **103,** 15 751–15 782.

Sexton, D. M. H., 2001: The effect of stratospheric ozone depletion on the phase of the Antarctic Oscillation. *Geophys. Res. Lett.,* **28,** 3697–3700.

Shindell, D. T., R. L. Miller, G. A. Schmidt, and L. Pandolfo, 1999: Simulation of recent northern winter climate trends by greenhouse-gas forcing. *Nature,* **399,** 452–455.

Smith, I. N., P. McIntosh, T. J. Ansell, C. J. C. Reason, and K. McInnes, 2000: Southwest western Australian winter rainfall and its association with Indian Ocean climate variability. *Int. J. Climatol.,* **20,** 1913–1930.

Stone, D. A., A. J. Weaver, and R. J. Stouffer, 2001: Projection of climate change onto modes of atmospheric variability. *J. Climate,* **14,** 3551–3565.

Stouffer, R. J., S. Manabe, and K. Bryan, 1989: Interhemispheric asymmetry in climate response to a gradual increase of atmospheric CO_2. *Nature,* **89,** 571–586.

Thompson, D. W. J., and J. M. Wallace, 1998: The Arctic Oscillation signature in the wintertime geopotential height and temperature fields. *Geophys. Res. Lett.,* **25,** 1297–1300.

——, and ——, 2000: Annular modes in the extratropical circulation. Part I: Month-to-month variability. *J. Climate,* **13,** 1000–1016.

——, and S. Solomon, 2002: Interpretation of recent Southern Hemisphere climate change. *Science,* **296,** 895–899.

Watterson, I. G., 2000: Southern midlatitude zonal wind vacillation and its interaction with the ocean in GCM simulations. *J. Climate,* **13,** 562–578.

Whetten, P. H., Z. Long, and I. N. Smith, 1997: Comparison of simulated climate change under transient and stabilised CO_2. BMRC Res. Rep. 69, Melbourne, Victoria, Australia, 96 pp.